

PAPER • OPEN ACCESS

Eden growth models for flat clathrin lattices with vacancies

To cite this article: Felix Frey *et al* 2020 *New J. Phys.* **22** 073043

View the [article online](#) for updates and enhancements.



PAPER

Eden growth models for flat clathrin lattices with vacancies

OPEN ACCESS

RECEIVED
29 March 2020REVISED
25 May 2020ACCEPTED FOR PUBLICATION
5 June 2020PUBLISHED
24 July 2020

Original content from
this work may be used
under the terms of the
[Creative Commons
Attribution 4.0 licence](#).

Any further distribution
of this work must
maintain attribution to
the author(s) and the
title of the work, journal
citation and DOI.

**Felix Frey^{1,2,5}** , **Delia Bucher³** , **Kem A Sochacki⁴** , **Justin W Taraska⁴** ,
Steeve Boulant³ and **Ulrich S Schwarz^{1,2,6}** ¹ Institute for Theoretical Physics, Heidelberg University, Philosophenweg 19, D-69120 Heidelberg, Germany² BioQuant Center for Quantitative Biology, Heidelberg University, Im Neuenheimer Feld 267, D-69120 Heidelberg, Germany³ Schaller Research Group at CellNetworks, Department of Infectious Diseases, Virology, University Hospital Heidelberg and German Cancer Research Center (DKFZ), Im Neuenheimer Feld 344, D-69120 Heidelberg, Germany⁴ National Heart Lung and Blood Institute, National Institutes of Health, Bethesda, MD 20892, United States of America⁵ Present address: Department of Bionanoscience, Kavli Institute of Nanoscience, Delft University of Technology, Van der Maasweg 9, NL-2629 HZ Delft, The Netherlands⁶ Author to whom any correspondence should be addressed.E-mail: schwarz@thphys.uni-heidelberg.de**Keywords:** stochastic dynamics, cluster growth, biological physics, endocytosisSupplementary material for this article is available [online](#)**Abstract**

Clathrin-mediated endocytosis is one of the major pathways by which cells internalise cargo molecules. Recently it has been shown that clathrin triskelion can first assemble as flat lattices before the membrane starts to bend. However, for fully assembled clathrin lattices high energetic and topological barriers exist for the flat-to-curved transition. Here we explore the possibility that flat clathrin lattices grow with vacancies that are not visible in traditional imaging techniques but would lower these barriers. We identify the Eden model for cluster growth as the most appropriate modeling framework and systematically derive the four possible variants that result from the specific architecture of the clathrin triskelion. Our computer simulations show that the different models lead to clear differences in the statistical distributions of cluster shapes and densities. Experimental results from electron microscopy and correlative light microscopy provide first indications for the model variants with a moderate level of lattice vacancies.

1. Introduction

Clathrin-mediated endocytosis (CME) is one of the major pathways by which cells internalise cargo molecules [1]. In CME clathrin triskelion assemble together with a layer of adaptor and accessory proteins in order to invaginate a patch of the cell membrane of several tens of nanometer radius [2]. The standard sequence of events are nucleation, growth and fission of the clathrin-coated structure [3, 4], but it is still unclear when exactly in this process curvature is acquired [5, 6]. Two opposing models have been proposed to explain how the clathrin coat evolves during the uptake process [7]. In the constant curvature model (CCM), the clathrin coat assembles with constant curvature [8]. As dictated by Euler's theorem, this requires the presence of twelve pentagons in the hexagonal lattice. The CCM implicitly assumes that these pentagons are incorporated in a continuous manner at the edge of the growing pit. In contrast, in the constant area model (CAM) the clathrin coat first assembles flat to finite size before the clathrin coat starts to bend [9]. Here pentagons have to get integrated either directly into the hexagonal lattice or they have to diffuse from the edge into the bulk of the lattice [10]. Both scenarios require major lattice rearrangements with high energetic and topological barriers [11]. First, multiple molecular bonds with binding energies of $\epsilon_{\text{clathrin}} = 23 k_B T$ per triskelion [12] would have to open up. Second, to add another face to the hexagonal lattice, one had to add exactly two triskelion to the existing lattice, which then would also create both pentagons and heptagons [13].

Although electron microscopy (EM) images show the existence of flat clathrin lattices [14], the CAM has been disfavoured for the energetic and topological reasons given above. However, recent experiments have

changed this picture. First, EM suggested that curvature is higher in more mature structures and that the patch area does not change much with curvature, lending strong support for the CAM [9]. Second, fluorescence recovery after photobleaching (FRAP) experiments have suggested that the clathrin coat is highly dynamic [9, 15–17]. This view was further supported by a quantitative study combining correlative light and electron microscopy (CLEM) and mathematical modelling, which suggested that the lattice first grows flat and starts to bend only after on average 70% of the clathrin content has been acquired [18]. Another recent study using polarised total internal reflection fluorescence microscopy has shown that different assembly pathways coexist, even within a single cell [19]. Together these recent developments suggest that the assembly pathway is more plastic than formerly appreciated, and that bending can sometimes occur at relatively late stages.

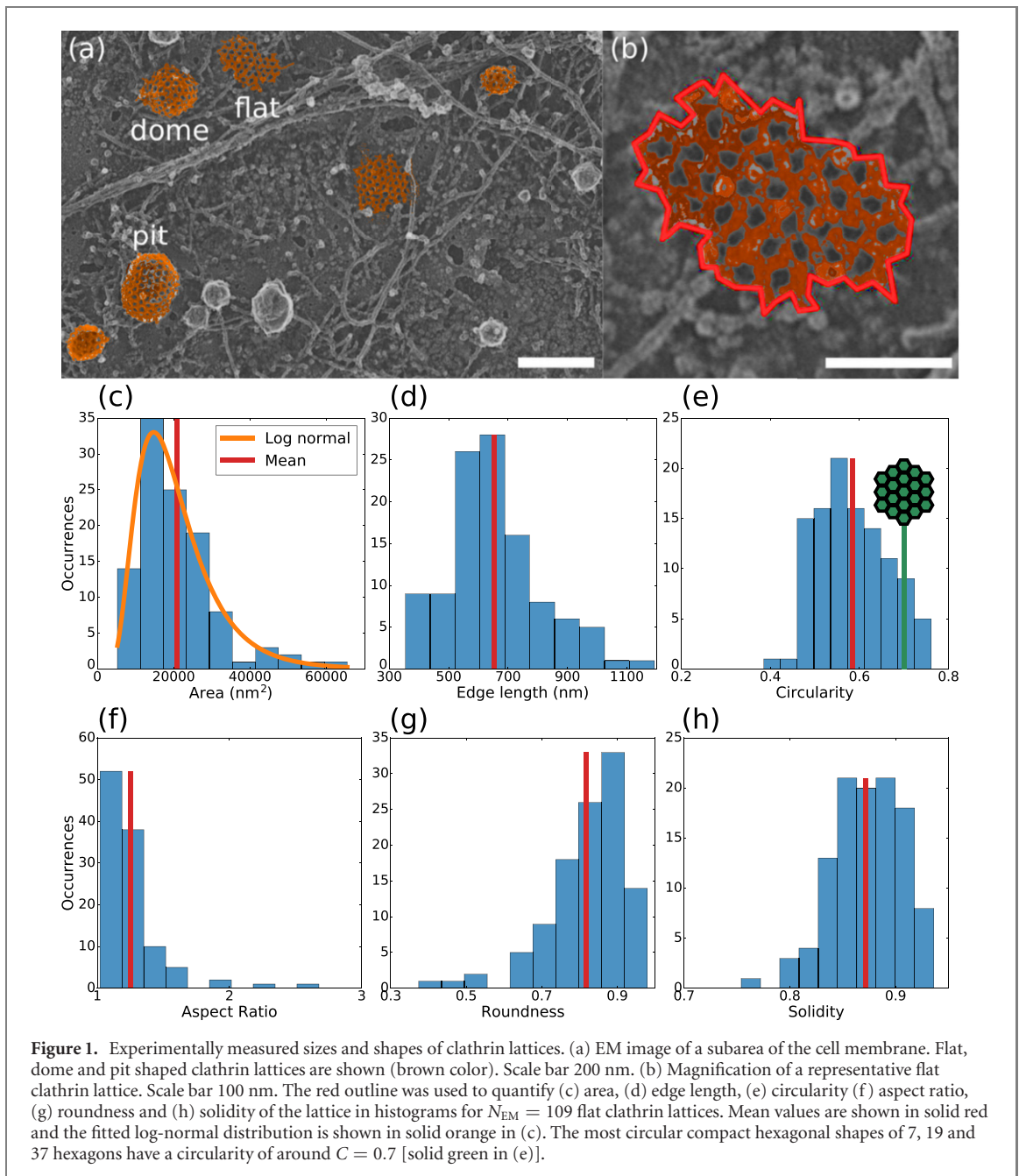
To address the essential question of how bending can become possible in a flat clathrin lattice, here we explore the possibility that hexagonal lattices might be less homogeneous than usually assumed and might contain a substantial fraction of vacancies. As lattice vacancies we define positions within the clathrin lattice where lattice sites are unoccupied, but which are distributed in the lattice such that binding triskelion to these vacancies would not change the number of occupied lattice edges. In contrast to pentagonal or heptagonal defects, which would be visible in standard visualisation methods (metal replica EM, cryo-EM with subtomogram averaging, atomic force microscopy), such lattice vacancies are currently very hard to detect directly with experimental methods (figure S1 <https://stacks.iop.org/NJP/22/073043/mmedia>). Therefore here we address this important question with a theoretical approach, which is informed and complemented by experimental data.

This work is structured as follows. We first consider different choices for a potential modeling framework for cluster growth with clathrin triskelion and identify the Eden model as the most appropriate one based on a statistical analysis of EM-images of flat clathrin lattices. Taking into account the specific architecture of the clathrin triskelion, we then define all four model variants that should be considered based on differential binding between the different clathrin domains. Using computer simulations, we find that these different models give distinct predictions for the statistical distribution of shapes and densities of clathrin lattices. We finally show that experimental data seem to favor the model classes with a moderate level of lattice vacancies, although at this stage our conclusions are not definite yet. We conclude that our newly developed Eden model for the growth of flat clathrin lattices is sufficiently detailed to explore different molecular binding scenarios, but also sufficiently efficient to obtain statistical results that can be compared with experimental data.

2. Results

We first addressed the question which modeling framework is most appropriate for the growth of flat clathrin lattices. To guide model selection and definition by experimental data, we performed experiments with a cell line (BSC-1) that is known to not develop large and long-lived flat lattices (plaques), but rather features many small flat lattices that eventually convert to curved pits [18]. In particular, these flat lattices are smaller than in other cell lines, e.g. HeLa-cells [16, 17]. We first analysed the size and shape of these flat clathrin structures on images with ultrastructural resolution. Figure 1(a) shows an EM image of a subregion of the cell membrane in which flat, dome and pit shaped clathrin lattices can be seen (marked in brown). In figure 1(b), a magnification of a typical flat clathrin lattice shows how the size and contour are determined. The outline or edge length (red) confines the lattice and was determined by marking points manually at the edge of the lattice with ImageJ [20]. These points are then connected by straight lines. By this choice the contour has the shape of a polygon. We follow this routine as it can be easily extended to computer simulations. Using these procedures, we obtained area (A) (figure 1(c)), edge length (L) (figure 1(d)), circularity ($C = 4\pi A/L^2$) (figure 1(e)), aspect ratio (length of major axis/length of minor axis) (figure 1(f)), roundness (inverse aspect ratio) (figure 1(g)) and solidity (area/convex area) (figure 1(h)) of the flat clathrin lattices.

Below we will use all these metrics to compare simulations and experiments, but the main focus will be on circularity C , which is easy to define in the simulations and has been used before to characterise clathrin lattices [16, 17]. While a perfect circle would have $C = 1$, all other structures will have smaller values. We note that the most circular compact hexagonal shapes of 7, 19 and 37 hexagons, which represent 13, 30 and 42 edges, respectively, have $C \approx 0.7$ (green line in figure 1(e)), where the area of a single hexagon is $A_0 = 796 \text{ nm}^2$ and the length of a single segment $L_0 = 17.5 \text{ nm}$ (see supplementary information, from now on referred to as SI). For most lattices the circularity is below this value, suggesting that the main source for the small C -value is not only the rugged rim, but the elliptical shape. Our results for aspect ratio, roundness and solidity confirm this conclusion. Regarding aspect ratio (figure 1(f)) we see that most of the clathrin lattices are rather compact, with aspect ratios around 1.5. Only very few clathrin lattices show an aspect

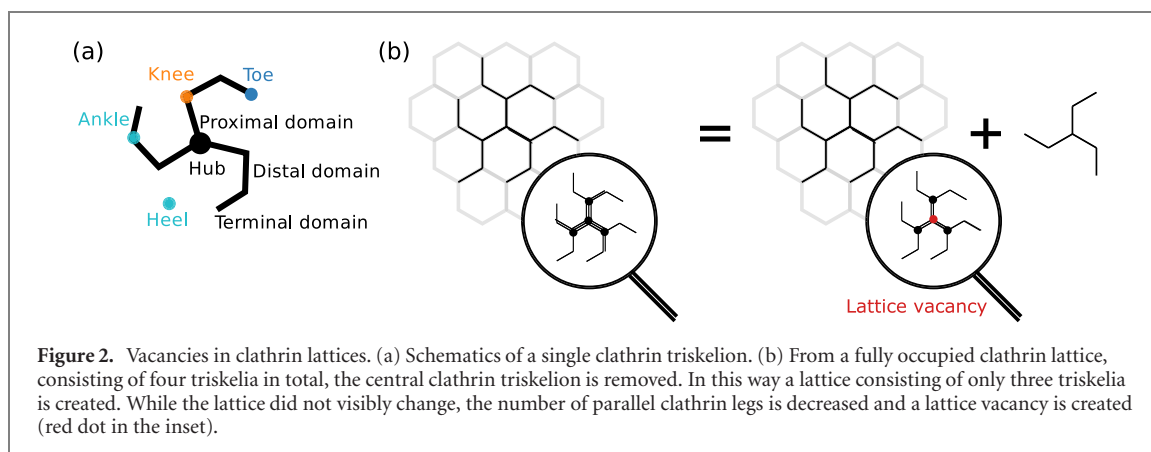


ratio that is larger than 2. Analysis of the roundness and solidity distribution of the clathrin lattices [figures 1(g) and (h), respectively] showed that the distribution is quite narrow and agrees well with the results for circularity.

The results from figure 1 reveal several important aspects of clathrin lattice growth that are essential for corresponding computer simulations. First, there is a distinct heterogeneity between individual lattices, resulting in a broad distribution and suggesting a stochastic model. Second, considering the circularity, it is obvious that the clathrin lattices are only in rough approximation circular. The low C -values suggest that this is only partly due to the hexagonal lattice leading to a rough contour, and that the clathrin lattices become anisotropic due to the underlying growth process. Thirdly, the area distribution can be approximated by a log-normal distribution [21]

$$f(A) = \frac{1}{\sqrt{2\pi\sigma^2 A}} \exp\left(-\frac{(\ln(A) - \mu)^2}{2\sigma^2}\right), \quad (1)$$

with $\exp(\mu)$ being the geometric mean and $\exp(\sigma)$ the geometric standard deviation, which together determine the shape of the distribution. The fit to the data is shown as solid orange line in figure 1(c). It gives $\mu = 9.8$ (corresponding to an area of $A = 18568 \text{ nm}^2$) and $\sigma = 0.48$. We note that the log-normal distribution is typical for random processes with multiplicative nature. In our case the area of the clathrin



lattices is given by the successive addition of clathrin triskelia such that the noisy incremental growth steps multiply, leading to a log-normal distribution. We conclude that clathrin lattices grow with a considerable level of stochasticity.

In order to develop a stochastic growth model, we next have to take into account the specific structure of the clathrin triskelion as shown schematically in figure 2(a). From the central hub, three legs emanate, each with three domains. The proximal and distal domains define the two possible overlap regions in the lattice, with nearest and next-nearest neighbors. The terminal domain is directed towards the membrane and binds adaptor and accessory proteins, so it does not contribute directly to the structural organisation of the lattice. In the following, we call the connection between proximal and distal domain the *knee*, the connection between distal and terminal domain the *ankle*, and the site at the end of the terminal domain the *toe*. Oriented oppositely to the ankle, but at the same distance from knee and hub, we define the *heel* position.

Next we consider the structure of a clathrin lattice that is built by several triskelia, as schematically shown in figure 2(b). We define *cluster nodes* as all nodes of the lattice that are occupied either by hubs, knees or ankles (in the cartoon all nodes that are connected by black legs). We define an *edge node* as a cluster node that is connected to an unoccupied node; this defines the edge of the clathrin cluster. Finally we define a *lattice vacancy* as a node that is not occupied by a triskelion hub, but whose occupancy would not change the number of cluster nodes. To further illustrate this concept, in figure 2(b) we consider a fully occupied clathrin lattice, consisting of four triskelia in total (left), from which the central clathrin triskelion is removed (right). In this way a lattice consisting of three triskelia is created. While the lattice did not visibly change, the number of parallel clathrin legs is decreased and a lattice vacancy is created (shown as red dot in the inset).

Regarding the dynamics of growth, in general one expects three different phases, namely a lag phase until a critical nucleus has been formed, then a phase of rapid growth and finally a saturation phase. Together this gives a sigmoidal growth curve in time, as known e.g. from the growth of virus capsids [22, 23]. The sigmoidal growth curve can be understood well with rate equations that describe the time evolution of the distribution of the sizes of the intermediates. The most general mathematical framework for this approach are the coagulation–fragmentation equations [24, 25]. If growth occurs only through addition or removal of monomers, one deals with the special case of the Becker–Döring equations [26, 27]. Importantly, in this framework of reversible growth, the saturation regime emerges as a balance of association and dissociation.

Although time traces of CME in general show this sigmoidal shape [18, 28], the conceptual framework here has to be different for several reasons. First, the formation of a critical nucleus is strongly determined by signaling and adaptor proteins like AP2. Second, the saturation regime is related to the formation and scission of the membrane neck and already convoluted with the movement of the forming vesicle into the cytoplasm. Therefore here we focus only on the intermediate regime of fast growth, which is characterized by fast addition of new clathrin triskelia to the growing lattice. In contrast to a rate equation approach, our emphasis is on the spatial aspects of growth and the role played by the peculiar geometry of the clathrin triskelia.

In general, the binding process of single units to a growing cluster can be limited either by diffusion or by reaction. The standard reaction-limited model for cluster growth is the Eden model. Originally introduced to study the growth of bacteria clusters [29], in this model the cluster is effectively growing from the inside, without any modeling of the transport required to bring in new components. In the Eden model a two-dimensional lattice is considered, that is initially occupied only by one lattice site. In the next step one

Table 1. Classification of models on full lattice.

Model name	Binding type	Binding order	Legs per edge	#Triskelia
KM	Hub at knee	1st	4	2
AM	Hub at ankle	2nd	2	1
HM	Hub at heel	2nd	2	1
TM	Hub at toe	3rd	1	3/5

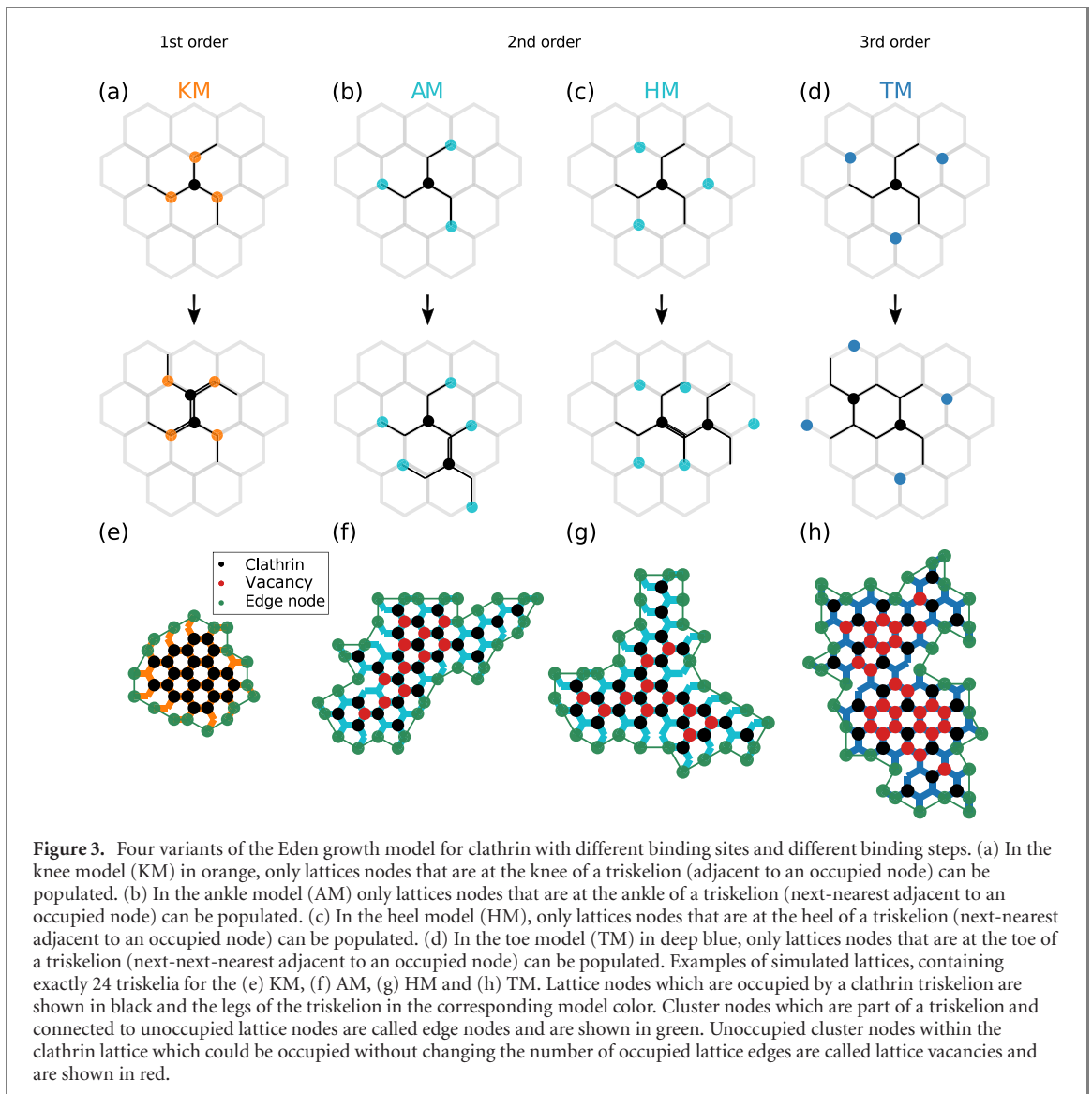
of the free neighboring lattice sites is chosen randomly with equal probability and the next site is populated. After neighboring lattice sites are updated the procedure starts over. This model results in compact shapes with limited contour roughness. The complementary model is diffusion-limited aggregation (DLA) [30], in which new material first has to diffuse towards the existing cluster, but upon encounter each new component sticks immediately at the new location. Thus a DLA-cluster is completely dominated by the transport process and has a fractal shape.

For clathrin lattice growth we expect that the concentration of unbound clathrin triskelia is high and that they distribute sufficiently well such that material transport is not limiting. We also expect that the reaction rate is relatively modest due to the extended and complex geometry of clathrin triskelia and the importance of adapter and accessory proteins. Given the general observation that clathrin structures do not exhibit fractal shapes [14], and our experimental data of the circularity and solidity distribution in figures 1(e) and (h), respectively, we thus expect the growth process to be reaction-limited. Since flat clathrin lattices grow along the plasma membrane, we require a two-dimensional reaction-controlled growth model that neglects the diffusion process. Thus, the Eden model is the most appropriate starting point.

The total binding energy per clathrin triskelion has been estimated to be $\epsilon_{\text{clathrin}} = 23 k_B T$ for clathrin pits [12]. Assuming a similar value for flat lattices and given that a single triskelion has six segments in the lattice (three legs, each with a proximal and a distal domain being part of the lattice), each segment binds with a few units of thermal energy to its environment. This suggests that after binding to the clathrin lattice, the triskelion can still rearrange itself. We also note that the triskelia cannot only attach to the edge of the growing lattice, but also in the bulk, again arguing that transport is not limiting. In order to account for the different degrees of heterogeneity of the growing lattices, we therefore aim at a Eden-type growth model that leads to compact shapes of varying internal density. We note that the clathrin system is especially suited to implement corresponding mechanisms because of the known domain substructure of the triskelia.

Informed by the internal geometry of hexagonal clathrin arrays, we now show that four different variants of the Eden growth model have to be considered. We classify the different growth models according to the distance with which new triskelia can bind with respect to the hub of an already present triskelion and thus distinguish between first, second and third order models (cf table 1). In the first row of figure 3, we show different initial configurations of our growth models, while the second row shows possible configuration after one growth step. The *knee model* (KM) (figure 3(a)) is of first order; here only lattice nodes that are at the knee of a triskelion (adjacent to an occupied node) can be populated (orange). Note that the KM can be considered to be the traditional view on clathrin lattice growth, leading to maximal density of the lattice. The *ankle model* (AM) (figure 3(b)) and the *heel model* (HM) (figure 3(c)) are of second order; here only lattice nodes that are at the ankle (or heel) of a triskelion (next-nearest adjacent to an occupied node) are possible binding sites (cyan). Finally, the *toe model* (TM) (figure 3(d)) is of third order; here only lattice nodes that are at the toe of a triskelion (next-next-nearest adjacent to an occupied node) can be populated (deep blue). These four growth models represent all possible modes of how clathrin lattices can grow dictated by the geometry and different binding affinities of the triskelion. All other choices are mixtures between these fundamental growth models or would lead to lattices that will not cover a hexagonal lattice completely. While each of the four growth models can be simulated with an Eden algorithm, they reflect different transport and binding processes which add new triskelia to the growing cluster.

For the simulation and analysis of growing clathrin lattices we have developed custom-written computer code [31] (details can be found in the SI). We first draw an area value A from the experimentally measured area distribution shown in figure 1(c). We then place new triskelia on a hexagonal lattice in the following manner. The simulation starts by choosing the initial position of the first clathrin triskelion. We assume that all triskelia have the same chirality, which reduces the number of possible attachment points [32]. The hub or node of the triskelion is shown as a black circle and the legs of the triskelion in the corresponding model color (compare figure 3). Next, a list of potential growth sites is defined by all nodes that are connected to the existing clathrin lattice (in the beginning: a single triskelion) but still unoccupied by a triskelion. From the list of potential growth sites a node is drawn uniformly. After the triskelion is placed into the lattice the

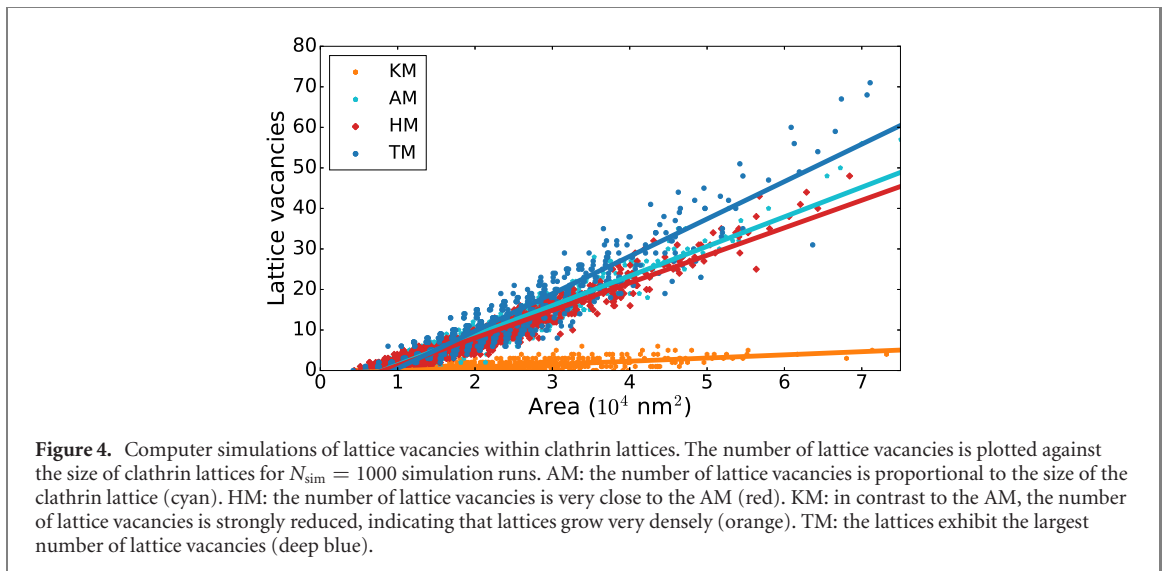


procedure starts again. This growth algorithm gives the same distribution of area A as determined experimentally [compare figure 1(c)]. Therefore, we can compare the shapes and densities of lattices of the different growth models, all with the same area distribution.

Figures 3(e)–(h) show examples of simulated clathrin lattices containing exactly 24 triskelia for the four Eden model variants KM, AM, HM and TM, where cluster nodes (black), edge nodes (green) and lattice vacancies (red) are shown. Since the growth algorithm is a stochastic process, the formed clathrin lattices differ in size and shape, and their geometrical properties have to be assessed in a statistical manner.

We first use our simulations to predict the heterogeneity of clathrin lattices, since lattice vacancies are hard to see with all standard visualisation techniques (compare figure S1). In figure 4 we show the number of lattice vacancies as a function of clathrin lattice size for the KM (orange), the AM (cyan), the HM (red) and the TM (deep blue). A linear fit to the data reveals that both quantities are strongly correlated, but with very different slopes. We determine the Pearson correlation coefficient to be $R_{\text{KM}} = 0.71$, $R_{\text{AM}} = 0.97$, $R_{\text{HM}} = 0.96$ and $R_{\text{TM}} = 0.95$. The number of lattice vacancies is very small in the KM, which can be considered to be the traditional view on compact clathrin lattices. In contrast, the AM and HM clearly show a higher level of lattice vacancies. We note that since the AM and the HM are equivalent regarding their structure, their results only differ due to statistical effects. Therefore, in the following we refrain from showing the results of the HM in the main text. Nevertheless, the results of the HM are included in the SI and all conclusions for the AM will also hold for the HM. Finally it follows from figure 4 that the TM has the highest level of lattice vacancies.

In figure 5, we compare our simulation results to the EM-data. In detail, we correlate circularity (figure 5(a)), edge length (figure 5(b)), solidity (figure 5(c)) and roundness (figure 5(d)) with the logarithm of the area for the EM-measurement for the KM, the AM and the TM. We immediately note that the



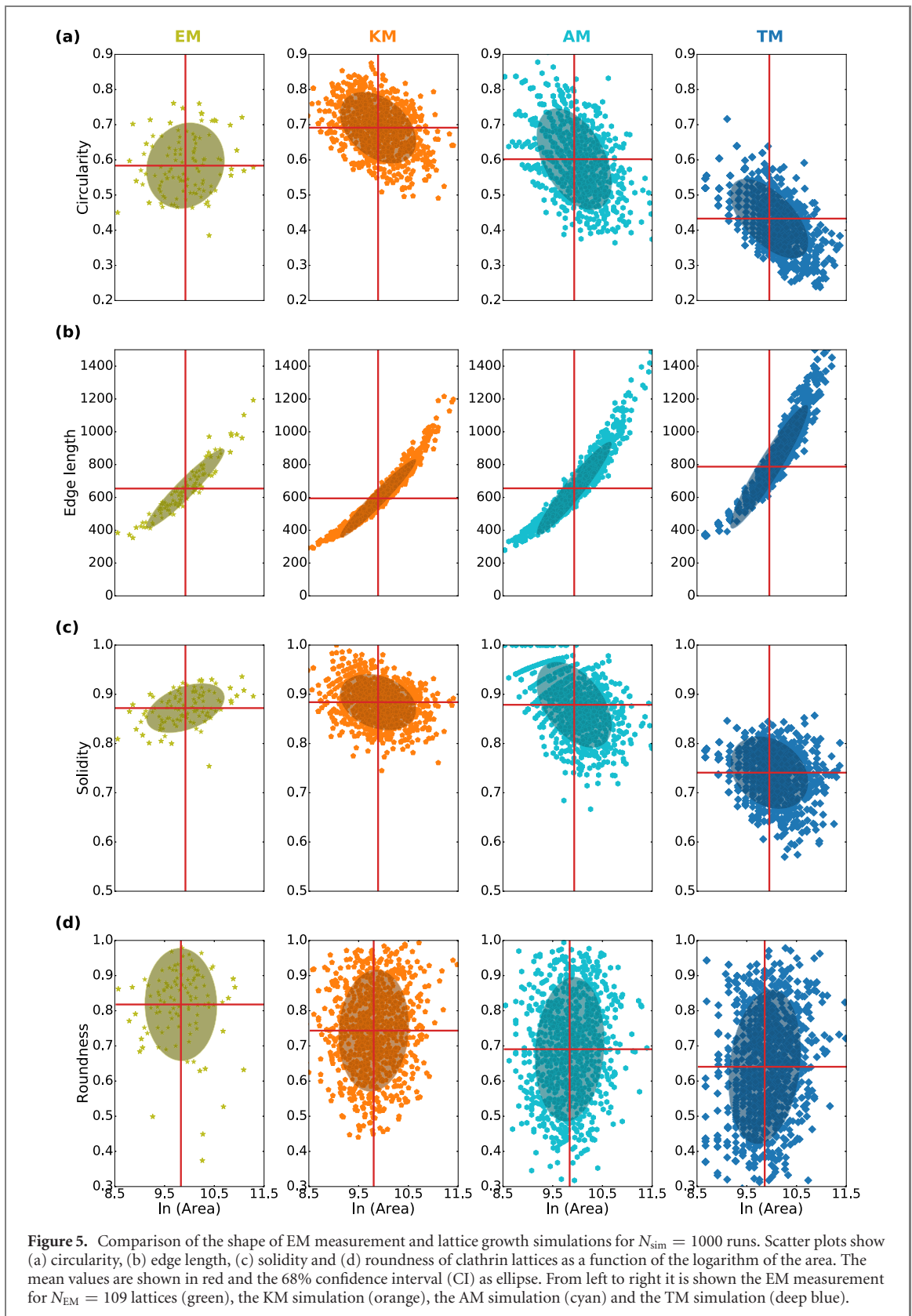
experimental data does not support the TM, because it deviates in regard to each metric. In contrast, the KM and AM deviate clearly only for circularity and solidity, respectively. As noted above, the HM gives very similar results compared to the AM (cf figure S2). Interestingly, the simulated data indicates that larger lattices seem to be less circular. We note that a recent experimental study using electron and super-resolution microscopy found a similar correlation between circularity and area of flat clathrin lattices, albeit for other cell types (HEK-293T and HeLa) which have much larger planar clathrin lattices [16]. Considering circularity and roughness in figures 5(a) and (c), we see that there are also discrepancies between the experimental data and the simulations at large areas. While the distribution of circularity is symmetric around the mean and the distribution of solidity increases with area in EM, both distributions decrease with area in the simulations. This finding could hint at another mechanism that comes into play during the progression of the assembly process, possibly mediated by the recruitment of additional proteins not considered in our model.

To compare our simulation results to another experimental data set, we use CLEM-data which correlate the fluorescent intensity of flat clathrin lattices immunostained for clathrin heavy chain and their size in EM (cf figure S3) [18]. Figure 6(a) shows for four cells that the intensity of the background corrected CLEM-data I scales linearly with the lattice area A , which in turn should scale linearly with the number N of triskelia and therefore with the protein mass of the lattice. However, the coefficient of proportionality between I and A as shown in figure 6(a) is different in each experiment, suggesting different labeling efficiencies and different imaging conditions in different experiments. Together these results suggest that the intensity can indeed be used as proxy for the number of triskelia N , but only after normalization within each experiment. Hence, the intensity relative to the mean intensity equals the number of clathrin triskelia relative to the mean number of clathrin triskelia

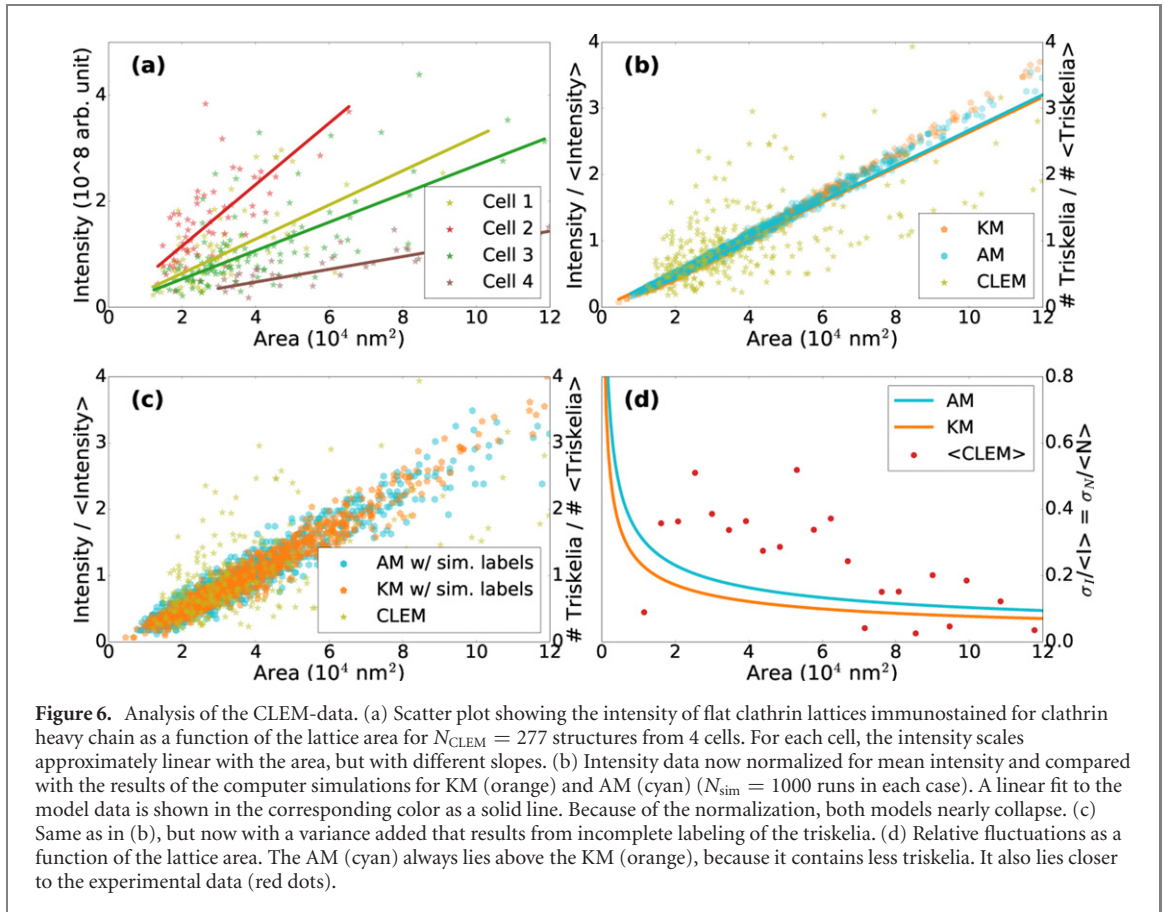
$$I(A) = \beta N(A) \rightarrow \frac{I(A)}{\langle I \rangle} = \frac{N(A)}{\langle N \rangle}, \quad (2)$$

where the constant of proportionality β drops out by normalisation. Figure 6(b) shows a scatter plot for all four cells of the intensity relative to the mean intensity as a function of the lattice area for the measured CLEM-data (green stars). At the same time, we plot the normalized results for the two remaining models, namely the KM (orange) and AM (cyan). Here we use the area distribution directly measured for the CLEM-data as given in figure S4. All data sets show similar scaling, which suggests that our models indeed can describe the CLEM-data. However, due to the normalization, the two models nearly collapse, thus it is not yet possible to distinguish between them at this point. Yet the normalization procedure revealed that the two models indeed are very different, because they required very different averages. First, a linear fit to the data ($N = \rho_m A$, shown in the corresponding color) reveals that the density ρ_m of the KM, $\rho_{\text{KM}} = 16.9/10^4 \text{ nm}^2$ is much larger than the density of the AM, $\rho_{\text{AM}} = 9.4/10^4 \text{ nm}^2$. Second, the mean number of triskelia is $\langle N_{\text{KM}} \rangle = 62$ and $\langle N_{\text{AM}} \rangle = 34$ for the KM and AM, respectively (the full distribution is provided as figure S5).

After the averages, we next discuss the variances in the fluorescence data and how they compare to our different Eden models. We first note that the simulated spread in figure 6(b) is very small compared with



the experimental data. The most reasonable explanation is that in the CLEM-data not every clathrin triskelion is immunostained for clathrin heavy chain. Due to this fact the fluorescence intensity can vary for clathrin lattices spanning across a similar area and containing a similar number of triskelia. To mimic this variation we simulate the number of labeled clathrin triskelia. We assume that each of the triskelia within a lattice of N triskelia has the probability p to be labeled. Then the probability that n out of N triskelia are labeled is given by a binomial distribution



$$P(n; N) = \binom{N}{n} p^n (1-p)^{N-n}. \quad (3)$$

By sampling the number of labeled clathrin triskelia we have a quantitative prediction of how strongly the intensity should vary. Figure 6(c) shows the results for the KM and AM, respectively (corresponding results for HM in figure S6). Here we use $p = 0.5$ as the choice with least bias. For CLEM with antibody labeling as used here, this is a reasonable value. The larger spread of the experimental data compared to the simulations could be either attributed to a smaller value of labeling probability p or experimental cell-to-cell variability. Regarding cell-to-cell variability we note that we here analyze only four cells, limited by the large effort to extract the geometry of clathrin lattices. We also note that we already have scaled out the overall fluorescence intensity from our data and thus we cannot use p anymore as a full fit parameter. Figure 6(c) shows that the variance added by this procedure is larger for the AM. This is easy to understand because the KM contains more triskelia and therefore the relative fluctuations compared to the mean are decreased. In detail, for the binomial distribution the mean and the standard deviation are given by $\langle N \rangle = Np$ and $\sigma_N = \sqrt{Np(1-p)}$, respectively. Hence

$$\sigma_I = \beta \sigma_N \rightarrow \frac{\sigma_I}{\langle I \rangle} = \frac{\sigma_N}{\langle N \rangle} = \sqrt{\left(\frac{1-p}{p}\right) \frac{1}{N}} = \sqrt{\left(\frac{1-p}{p}\right) \frac{1}{\rho_m A}}, \quad (4)$$

where the proportionality factor β drops out and where we used in the last step that the number of triskelia N is given by the area A and density ρ_m (dependent on the model) of the lattice. Because ρ_m is smaller for the AM, it will always give larger fluctuations than the KM. While the left-hand side of equation (4) can be measured from the CLEM-experiments, the right-hand side can be calculated for the KM and AM. For this purpose, we bin the CLEM-data for every cell according to their lattice area, and calculate standard deviation and mean for every bin (compare SI). In figure 6(d) we finally plot the mean for every bin (red dots). The KM and AM model are shown in orange and cyan, according to equation (4). Both models show the same decreasing trend as the experimental data and the AM seems to be a bit closer to the data points than the KM, which in turn would correspond to an intermediate level of lattice vacancies.

3. Discussion

Here we have addressed the hypothesis that flat clathrin lattices might be more spatially heterogeneous than formerly appreciated. Pentagonal or heptagonal defects and even broken lattices are often found in flat clathrin lattices, but here we address another type of potential defect, namely lattice vacancies that arise because the triskelia might not be close-packed in a flat hexagonal lattice. A closed-packed arrangement would correspond to a lattice for which every vertex is occupied by a clathrin triskelion without having any lattice vacancies. In our approach, this traditional view corresponds to the KM. However, here we also have formulated alternative models, namely the AM, HM and TM, that would allow for less dense lattices and more lattice vacancies. The spatial heterogeneity of clathrin lattices caused by lattice vacancies could explain the observed high exchange dynamics and plasticity with regard to bending.

The lattice vacancies addressed here could occur in hexagonal lattices that upon visual inspection look regular and close-packed. In standard light microscopy, they would not be directly detectable due to the resolution limit. Moreover lattice vacancies are currently challenging to see in metal replica EM or cryo-EM at the single vesicle level. Single molecule fluorescent microscopy or atomic force microscopy (AFM) applied to clathrin lattices [33–35] might have the required resolution, but have not yet been used to investigate this question. In addition, the results of cryo-EM and AFM studies are difficult to interpret, especially since the structural analysis is often a result of spatial averaging that will obscure spatial heterogeneity (cf figure S1) [33, 36, 37].

In order to quantify the level of spatial heterogeneity that arises from the peculiar geometry of the clathrin triskelia during the phase of rapid growth, here we have derived four different model variants based on the Eden model for growth of compact clusters. Because we focus on spatial aspects, a rate equation approach as often employed for reversible growth of supramolecular assemblies such as spherical virus capsids [22, 23] or linear assemblies [27] seems less appropriate, although it would be able to represent the full sigmoidal shape of the growth traces. In the future, our coarse-grained approach can be augmented by more microscopic details, using e.g. particle-based simulation models such as coarse-grained molecular dynamics [38] or Brownian dynamics [11, 39].

The four different Eden models arise from the specific architecture of the clathrin triskelion (three domains connected by two joints, the knee and the ankle, which correspond to potential binding sites of the hubs of other triskelia) and lead to different predictions regarding the statistical distribution of cluster sizes and shapes. The four model variants should be considered to represent the four principal growth modes of the system; in principle, one could also consider mixtures of these variants. However, in the absence of experimental data on the exact mechanism of binding, such extensions would lead to additional unknown model parameters. While we leave the systematic study of model mixture to future work, we here only considered one possible case, in which binding both to the knee and ankle of clathrin triskelia is allowed. However, the results of the knee-and-ankle model (KAM) do not show significantly increased agreement between the experimental data and the simulations (figures S7 and S8).

By comparing the four different fundamental growth models to experimental data, we found first evidence pointing towards a moderate level of lattice vacancies as predicted by the AM. In the AM, new triskelia only bind to binding sites at the ankle of clathrin legs. This suggests that incoming triskelia are more likely to be bound at the more distal parts, either due to special transport modes or due to increased binding energies. The AM suggests that proximal domains of clathrin triskelia do not bind well to each other in the flat state. We therefore predict that binding of proximal and distal domains is more favourable in the flat state, in contrast to the predictions of the KM, which presents the traditional view in which proximal domains bind to each other. Our predictions agree with the notion that in assembled hexagonal barrels, proximal domains do not align [36]. The suggested binding of proximal and distal domains leads to a longer lever between adjacent triskelia, which is also in agreement with the notion that clathrin structures adapt their conformation by gently flexing their legs [37].

Although we only make predictions on how flat lattices grow, our results support the notion that clathrin lattices first grow flat before they start to bend [9, 18, 19], since the lattice vacancies predicted here could create space and reduce entanglement of the clathrin lattice. As a consequence, this space can lead to the observed high degree of clathrin exchange [9, 16, 17] and the reduced entanglement can facilitate the insertion of new triskelia into the lattice to create pentagons (since it will be energetically less costly), which is a prerequisite for lattice bending [9, 18, 19]. Our prediction of lattice vacancies provides an appealing basis for future work on the detailed mechanisms of bending.

Given that our model is specifically developed for rapid growth due to the special architecture of the triskelia and naturally uses the KM of almost fully occupied lattices as reference case for the other model variants, we did not consider the potential role of unbinding, which in principle could further increase spatial heterogeneity. Although the high dynamics observed in FRAP is an important motivation for our

work [9], there is some debate about the exact interpretation of these results, including the limitations in optical microscopy to spatially separate traces and the possibility that only parts of the clathrin-complex is undergoing exchange. In the absence of more experimental data on potential unbinding processes in the clathrin lattice, it is challenging to develop a realistic model for this important aspect, which however should be addressed in future work.

Despite these caveats, the high degree of clathrin exchange is also another hint for the existence of lattice vacancies. Taking snapshots of a lattice with clathrin exchange would necessarily reveal a lattice with lattice vacancies because a lattice that is fully occupied at each point in time cannot exhibit turnover. Importantly, the turnover of flat clathrin lattices is stronger compared to the exchange of curved ones shown using an *in vitro* system [33]. Since new triskelia have to be added for generation of the required pentagons, the density of clathrin triskelia should increase in late stages, which is in agreement with recent observations [40]. An important question in this context is whether lattice vacancies are also present in longer-lived clathrin plaques. However, since these structures are very limited in the cell line which was used in this study (BSC-1) under our growth conditions, it has to be addressed by future work.

Our results agree with the emerging view that clathrin lattices are highly plastic and regulated by cellular factors, such that curvature can be built up once some cellular checkpoint has been cleared [4, 6]. We also note that bending based on lattice vacancies would first increase density and then stop polymerisation, thus providing a simple physical mechanism to proceed in the standard sequence of CME. Our results also agree with the suggestion that a typical maturation time leads to a typical patch size, around which a statistical distribution exists [41]. We also speculate that vacancies in the flat lattice could act as binding sites for signalling molecules, regulatory proteins, or cargo. In general, if lattice vacancies existed in clathrin lattices as predicted here, this would open up many new avenues for controlling their biological function.

Data availability

All datasets are available from the authors upon request. The computer code for the simulation of clathrin lattice growth has been deposited on GitHub [31].

Acknowledgments

FF acknowledges support by the Heidelberg Graduate School of Fundamental Physics (HGSFP). DB acknowledges support by a fellowship of the Heidelberg Biosciences International Graduate School (HBIGS) and by a travel Grant from Boehringer Ingelheim Fonds (BIF). USS and SB are members of the Collaborative Research Center 1129 of the German Research Foundation (DFG) funded under Projektnummer 240245660. SB was supported by a research Grant from the Chica and Heinz Schaller Foundation and by the Heisenberg program of the DFG (project number 415089553). JWT acknowledges support by the Intramural Research Program of the National Heart Lung and Blood Institute, National Institutes of Health, U.S.A. We would like to thank the US National Heart Lung and Blood Institute (NHLBI) Electron Microscopy Core and Light Microscopy Core facilities for use of equipment.

ORCID iDs

Felix Frey  <https://orcid.org/0000-0001-8501-6017>
Kem A Sochacki  <https://orcid.org/0000-0003-1160-4558>
Justin W Taraska  <https://orcid.org/0000-0001-5355-9535>
Steeve Boulant  <https://orcid.org/0000-0001-8614-4993>
Ulrich S Schwarz  <https://orcid.org/0000-0003-1483-640X>

References

- [1] Alberts B, Johnson A, Lewis J, Morgan D, Raff M, Roberts K and Walter P 2015 *Molecular Biology of the Cell* 6th edn (New York: Garland Science)
- [2] Kaksonen M and Roux A 2018 *Nat. Rev. Mol. Cell Biol.* **19** 313–26
- [3] Picco A and Kaksonen M 2018 *Curr. Opin. Cell Biol.* **53** 105–10
- [4] Mettlen M, Chen P H, Srinivasan S, Danuser G and Schmid S L 2018 *Annu. Rev. Biochem.* **87** 871–96
- [5] Lampe M, Vassilopoulos S and Merrifield C 2016 *J. Struct. Biol.* **196** 48–56
- [6] Sochacki K A and Taraska J W 2019 *Trends Cell Biol.* **29** 241–56

- [7] Haucke V and Kozlov M M 2018 *J. Cell Sci.* **131** 216812
- [8] Kirchhausen T 1993 *Curr. Opin. Struct. Biol.* **3** 182–8
- [9] Avinoam O, Schorb M, Beese C J, Briggs J A and Kaksonen M 2015 *Science* **348** 1369–72
- [10] Pearse B M F and Bretscher M S 1981 *Annu. Rev. Biochem.* **50** 85–101
- [11] den Otter W K and Briels W J 2011 *Traffic* **12** 1407–16
- [12] Saleem M, Morlot S, Hohendahl A, Manzi J, Lenz M and Roux A 2015 *Nat. Commun.* **6** 1–10
- [13] Jin A J and Nossal R 1993 *Biophys. J.* **65** 1523–37
- [14] Heuser J 1980 *J. Cell Biol.* **84** 560–83
- [15] Wu X, Zhao X, Baylor L, Kaushal S, Eisenberg E and Greene L E 2001 *J. Cell Biol.* **155** 291–300
- [16] Grove J, Metcalf D J, Knight A E, Wavre-Shapton S T, Sun T, Protonotarios E D, Griffin L D, Lippincott-Schwartz J and Marsh M 2014 *Mol. Biol. Cell* **25** 3581–94
- [17] Maib H, Ferreira F, Vassilopoulos S and Smythe E 2018 *J. Cell Biol.* **217** 4253–66
- [18] Bucher D et al 2018 *Nat. Commun.* **9** 1109
- [19] Scott B L et al 2018 *Nat. Commun.* **9** 419
- [20] Schneider C A, Rasband W S and Eliceiri K W 2012 *Nat. Methods* **9** 671–5
- [21] Crow E L and Shimizu K 1987 *Lognormal Distributions: Theory and Applications* (New York: Marcel Dekker)
- [22] Zlotnick A 2005 *J. Mol. Recognit.* **18** 479–90
- [23] Hagan M F 2014 *Adv. Chem. Phys.* **155** 1–68
- [24] Wattis J A 2006 *Physica D* **222** 1–20
- [25] Da Costa F 2015 *Mathematical Aspects of Coagulation-Fragmentation Equations Mathematics of Energy and Climate Change* (Cham: Springer) pp 83–162
- [26] Ball J M, Carr J and Penrose O 1986 *Commun. Math. Phys.* **104** 657–92
- [27] Markvoort A J, ten Eikelder H M M, Hilbers P A J and de Greef T F A 2016 *ACS Cent. Sci.* **2** 232–41
- [28] Schöneberg J, Dambournet D, Liu T L, Forster R, Hockemeyer D, Betzig E and Drubin D G 2018 *Mol. Biol. Cell* **29** 2959–68
- [29] Eden M 1961 *Proceedings of the Fourth Berkeley Symposium on Mathematical Statistics and Probability, Volume 4: Contributions to Biology and Problems of Medicine*, (Berkeley, CA: University of California Press) pp 223–39
- [30] Witten T Jr and Sander L M 1981 *Phys. Rev. Lett.* **47** 1400–3
- [31] Frey F and Schwarz U S 2020 Python code for computer simulations of growing clathrin lattices <https://github.com/usschwarz/ClathrinLattices>
- [32] den Otter W K, Renes M R and Briels W J 2010 *Biophys. J.* **99** 1231–8
- [33] Dannhauser P N, Platen M, Böning H, Ungewickell H, Schaap I A and Ungewickell E J 2015 *Traffic* **16** 519–33
- [34] Usukura E, Narita A, Yagi A, Ito S and Usukura J 2016 *Sci. Rep.* **6** 27472
- [35] Yoshida A, Sakai N, Uekusa Y, Imaoka Y, Itagaki Y, Suzuki Y and Yoshimura S H 2018 *PLoS Biol.* **16** e2004786
- [36] Fotin A, Cheng Y, Sliz P, Grigorieff N, Harrison S C, Kirchhausen T and Walz T 2004 *Nature* **432** 573–9
- [37] Morris K L et al 2019 *Nat. Struct. Mol. Biol.* **26** 890–8
- [38] Matthews R and Likos C N 2013 *Soft Matter* **9** 5794–806
- [39] Mehraeen S, Cordella N, Yoo J S and Spakowitz A J 2011 *Soft Matter* **7** 8789–99
- [40] Sochacki K A, Dickey A M, Strub M P and Taraska J W 2017 *Nat. Cell Biol.* **19** 352–61
- [41] Kumar G and Sain A 2016 *Phys. Rev. E* **94** 062404